IEEE Access
Multidisciplinary ⋮ Rapid Review ⋮ Open Access Journal

Received September 21, 2020, accepted October 8, 2020, date of publication October 14, 2020, date of current version October 28, 2020.

Digital Object Identifier 10.1109/ACCESS.2020.3031032

A Reflective-Mode Phase-Variation Displacement Sensor

JONATHAN MUÑOZ-ENANO[1], (Graduate Student Member, IEEE), PARIS VÉLEZ[1], (Member, IEEE), LIJUAN SU[1], MARTA GIL-BARBA[2], (Member, IEEE), AND FERRAN MARTÍN[1], (Fellow, IEEE)

[1]GEMMA/CIMITEC, Departament d'Enginyeria Electrònica, Universitat Autònoma de Barcelona, 08193 Bellaterra, Spain
[2]Departamento Ingeniería Audiovisual y Comunicaciones, Universidad Politécnica de Madrid, 28031 Madrid, Spain

Corresponding author: Jonathan Muñoz-Enano (jonatan.munoz@uab.cat)

This work was supported in part by the MINECO-Spain under Project TEC2016-75650-R and Project PID2019-103904RB-I00, in part by the Generalitat de Catalunya under Project 2017SGR-1159, in part by the Institució Catalana de Recerca i Estudis Avançats (who awarded Ferran Martín), and in part by the FEDER funds. The work of Jonathan Muñoz-Enano was supported by the Secreteraria d'Universitats i Recerca (Gen. Cat.) and European Social Fund for the FI grant. The work of Paris Vélez was supported by the Juan de la Cierva Program under Project IJCI-2017-31339.

ABSTRACT In this paper, a displacement sensor based on an open-ended step-impedance transmission line is reported. The sensor operates in reflection, and the output variable is the phase of the reflection coefficient. The static part of the sensor is the step-impedance transmission line, where the open-ended line section is the sensitive part (sensing line). The movable part is a dielectric slab, e.g., an uncladded microwave substrate. When such slab, located on top of the sensing line, is in relative motion to the line, in the direction of the line axis, the portion of the sensing line covered by the slab varies, and this results in a change in the phase of the reflection coefficient of the line. The step impedance discontinuity contributes to optimize the sensor sensitivity, the key parameter. A detailed analysis providing the design guidelines is carried out and used to design a prototype displacement sensor. The characterization of the fabricated device points out the potential of the approach to implement highly sensitive displacement sensors. The sensor is a one-port device and operates at a single frequency.

INDEX TERMS Displacement sensor, microstrip, microwave sensor, phase-variation sensor, step-impedance transmission line.

I. INTRODUCTION

There are several strategies for the measurement of linear and angular displacements using microwaves. One of such strategy exploits frequency variation, where, typically, the relative motion between the static and the movable part of the sensor perturbs the resonance frequency (the output variable) of a planar resonant element [1]–[6]. One of the main limitations of frequency variation sensors (as such sensors are usually referred to) is the requirement of a wideband signal for measuring purposes. The spectrum of such signal must cover, at least, the output dynamic range. Thus, the generation of such signals may represent a penalty (in terms of the cost of the associated electronics) for sensor implementation in a real scenario.

The associate editor coordinating the review of this manuscript and approving it for publication was Flavia Grassi.

Single-frequency sensors constitute a good alternative to frequency variation sensors in order to reduce sensor costs. Among them, substantial investigation has been devoted to the so-called coupling modulation sensors [7]–[15]. Such sensors belong to the category of symmetry-based sensors, and consist of a transmission line symmetrically loaded with a symmetric resonator, in relative motion to the line. By choosing the line and the resonant element with symmetry planes of different electromagnetic sort, i.e., one being a magnetic wall and the other one an electric wall, line-to-resonator coupling is prevented, and (roughly) total transmission at the resonance frequency of the movable resonator is expected. However, by disrupting symmetry by means of a linear displacement or rotation, the coupling between the line and the resonator is activated, thereby reducing the magnitude of the transmission coefficient [5], [16], [17]. Since the intensity of coupling depends on the level of asymmetry (intimately related to the relative displacement between the line and the resonator),

the approach can be used for displacement sensing. In these sensors, the output variable is typically the magnitude of the transmission coefficient [7], [8]. However, by injecting a harmonic signal to the line, the displacement correlates to the magnitude of the envelope function of the amplitude modulated (AM) signal generated at the output port of the line [11], [12], [15].

It should be mentioned that there are other angular and linear displacement and velocity sensors, based on pulses, which exploit coupling modulation, as well. In these sensors, designated as electromagnetic encoders [18]–[22], the static part is also a transmission line, whereas the movable part is a chain (linear or circular) of metallic or dielectric inclusions (typically, although not necessarily, resonators). When the chain is in motion, in close proximity to the static line, the transmission coefficient of the line at the operating frequency is periodically modulated by the chain inclusions, with the result of a periodic envelope function, with pulses, at the output port. From the cumulative number of pulses and the time lapse between adjacent pulses, the linear, or angular, displacement and velocity can be inferred [18], [19].

Despite the fact that coupling modulation sensors operate at a single frequency, their robustness against noise is limited [17]. Nevertheless, the functionality of electromagnetic encoders as a low-cost alternative to optical encoders has been demonstrated [21], [23], [24]. An additional advantage of electromagnetic encoders over their optical counterparts is the possibility to operate in environments subjected to harsh and hostile conditions (i.e., with dirtiness, grease, pollution, etc.). Concerning coupling modulation sensors based on symmetry disruption (and exploiting typically a single sensing resonator), besides noise, an additional potential limitation concerns resonator detuning, which may limit the output dynamic range and sensitivity.

To alleviate the previous drawbacks of single-frequency coupling modulation sensors, phase variation sensors have been reported [25]–[29] (phase measurements are preferred over amplitude measurements in terms of noise). Phase variation sensors have been applied to the dielectric characterization of solid and liquids [25]–[27]. In such application, the working principle is the variation of the effective dielectric constant of a sensing line loaded with the material under test (MUT), which in turn modifies the phase of the line. The measurement of linear or angular displacements exploiting phase variation has also been demonstrated [28], [29]. For instance, in [28], the proposed sensor, based on a transmission line loaded with a rotating complementary split ring resonator (CSRR), takes advantage of the asymmetry of the sensor geometry and measures the angle of rotation in terms of the change in the relative phase of the reflection coefficients. A similar approach was presented in [29], where the difference in the phase of the reflection coefficients of a slotline loaded with a rotatable SRR is the output variable (nevertheless, most SRR and CSRR based sensors have been applied to dielectric characterization [30]–[32]). In [28], [29], two-port measurement are required. In this paper, we report a single-frequency reflective-mode phase-variation sensor devoted to the measurement of linear displacements between the static part, an open-ended (i.e., one-port) step-impedance transmission line, and the movable part, a dielectric slab (other reflective-mode sensors, mainly devoted to material characterization, have been recently reported [33]–[36]). Sensor sensitivity, i.e., the variation of the phase of the reflection coefficient with the linear displacement, is high, by virtue of the step-impedance discontinuity. Moreover, sensor functionality is based on a simple one-port (phase) measurement, and sensor fabrication is very simple, as far as the main elements, the static and the movable parts, are simply an open-ended step-impedance microstrip line and a dielectric slab, respectively.

Other approaches for sensing angular displacements have been reported (e.g., sensors based on circularly polarized antennas [37], magnetic microrods [38],[39] signal-interference transversal filtering sections [40], etc.), however, the complexity of these systems is by far superior to the one of the phase variation sensors reported in this paper.

Paper organization is as follows. In Section II, the structure, the working principle, and a detailed analysis of the proposed sensor (useful for design purposes), are reported. Using the resulting design guidelines of such analysis, a prototype sensor has been designed and fabricated. The designed and fabricated prototype are presented in Section III, also devoted to the experimental validation of the sensor. A discussion on sensitivity enhancement is reported in Section IV. A comparative analysis with other planar microwave displacement sensors is included in Section V. Finally, the main conclusions of the work are highlighted in Section VI.

II. SENSOR STRUCTURE, WORKING PRINCIPLE AND ANALYSIS

The proposed phase-variation displacement sensor consists of two parts: a static part and a movable part. The static part is an open-ended step-impedance transmission line, where the open-ended section is the sensitive part (Fig. 1). The movable part is a dielectric slab in relative motion to the static part. Specifically, the sensor is devoted to the measurement of linear displacement of the slab in the direction of the line axis, and this can be achieved by measuring the phase of the reflection coefficient of the step-impedance open-ended line. The working principle is the variation of the phase of the sensing line experienced when the dielectric slab moves in the axial direction. This modifies the phase of the reflection coefficient seen from the input port, the input variable.

Indeed, the effective dielectric constant of the sensing line is different (larger) in the region covered by the slab. Therefore, we can consider the sensing line as formed by two sections with variable length, i.e., the uncovered and the covered section (see Fig. 2). Let us designate by l the total length of the sensing line and by l_d and l_a the lengths of the covered and uncovered regions, respectively (so that $l = l_d + l_a$). The phase constant and the characteristic impedance of the

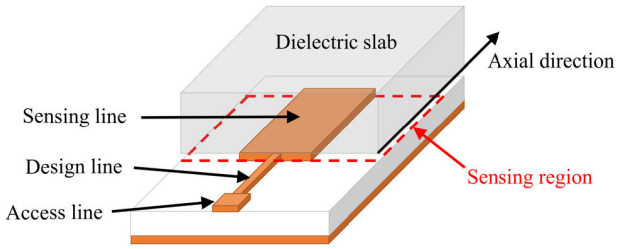

FIGURE 1. Sketch in perspective view of the proposed phase-variation displacement sensor.

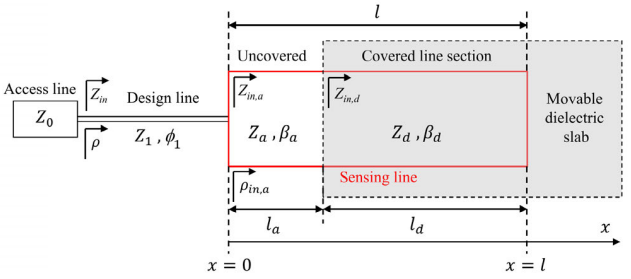

FIGURE 2. Detail (top view) of the proposed phase-variation displacement sensor and relevant parameters.

sensing line are also different in the covered and uncovered regions. Let us call these phase constants β_a and β_d, and the impedances Z_a and Z_d, where the sub-indexes a and d are used to distinguish whether the line is uncovered (air) or covered (dielectric).

The impedance, $Z_{in,d}$, seen from the plane separating the covered and uncovered line sections, and looking at the open end (Fig. 2), can be expressed as

$$Z_{in,d} = -jZ_d \cot(\beta_d l_d) \tag{1}$$

This impedance is the load of the uncovered line section, with input impedance given by

$$Z_{in,a} = \frac{jZ_a\left(Z_a \tan(\beta_a(l-l_d)) - Z_d \cot(\beta_d l_d)\right)}{Z_a + Z_d \cot(\beta_d l_d)\tan(\beta_a(l-l_d))} \tag{2}$$

Note that (2) has been expressed in terms of the input displacement variable, l_d.

Let us first consider the sensor as formed only by the sensing line, and let us infer the conditions for sensitivity optimization by considering the phase of the reflection coefficient as the output variable. The reflection coefficient is given by

$$\rho_{in,a} = \frac{Z_{in,a} - Z_0}{Z_{in,a} + Z_0} \tag{3}$$

where Z_0 is the reference impedance of the port. Introducing (2) in (3), the following result is obtained (4), as shown at the bottom of the next page and the phase of the reflection coefficient is

$$\phi_{\rho_{in,a}} = 2\arctan\left(\frac{Z_a(Z_d \cot(\beta_d l_d) - Z_a \tan(\beta_a(l-l_d)))}{Z_0(Z_a + Z_d \tan(\beta_a(l-l_d))\cot(\beta_d l_d))}\right) \tag{5}$$

The sensitivity, S, given by the derivative of $\phi_{\rho in,a}$ with l_d, can be expressed as

$$S = \frac{2}{1+\left(\frac{N}{D}\right)^2} \cdot \frac{D \cdot P - N \cdot Q}{D^2} \tag{6}$$

where N and D are the numerator and the denominator, respectively, of the argument of the arctan in (5), and P and Q are

$$P = -\frac{Z_a Z_d \beta_d}{\sin^2(\beta_d l_d)} + \frac{Z_a^2 \beta_a}{\cos^2(\beta_a(l-l_d))} \tag{7}$$

$$Q = -Z_0 Z_d \left\{\frac{\beta_a \cot(\beta_d l_d)}{\cos^2(\beta_a(l-l_d))} + \frac{\beta_d \tan(\beta_a(l-l_d))}{\sin^2(\beta_d l_d)}\right\} \tag{8}$$

The sensitivity in the limit when l_d approaches l (or $x = 0$) is found to be (9), as shown at the bottom of the next page In order to obtain the optimum line length, l, for sensitivity optimization, the derivative of (9) with l is obtained. After a straightforward (but tedious) calculation, the following expression results (10), as shown at the bottom of the next page. The zeros of (10), where the sensitivity, S_l, is either a maximum or a minimum, are obtained for those values of line length satisfying $\beta_d l = n \cdot \pi$ or $\beta_d l = (2n+1)\cdot\pi/2$, (with $n = 1, 2, 3\ldots$). By introducing these values of $\beta_d l$ in (9), the corresponding sensitivities are found to be:

$$S_l = 2Z_0 \left\{\frac{\beta_a}{Z_a} - \frac{\beta_d}{Z_d}\right\} \tag{11a}$$

for $\beta_d l = n \cdot \pi$, and

$$S_l = \frac{2}{Z_0}\left\{Z_a\beta_a - Z_d\beta_d\right\} \tag{11b}$$

for $\beta_d l = (2n+1)\cdot\pi/2$.

Let us now calculate the second derivative of (10) evaluated at $\beta_d l = n \cdot \pi$ and $\beta_d l = (2n+1)\cdot\pi/2$ in order to determine if the sensitivity is either a maximum or a minimum at these phase points. The results are:

$$\frac{d^2 S_l}{dl^2} = \frac{4Z_0\beta_d^2}{Z_d^3}\left\{(Z_a Z_d - Z_d Z_0^2 Z_a^{-1})\beta_a + (Z_0^2 - Z_d^2)\beta_d\right\} \tag{12a}$$

for $\beta_d l = n \cdot \pi$, and

$$\frac{d^2 S_l}{dl^2} = -\frac{4Z_d\beta_d^2}{Z_0^3}\left\{(Z_a Z_d - Z_d Z_0^2 Z_a^{-1})\beta_a + (Z_0^2 - Z_d^2)\beta_d\right\} \tag{12b}$$

for $\beta_d l = (2n+1)\cdot\pi/2$. Inspection of (12a) and (12b) reveals that the second derivative at the considered phase points exhibits different sign. Consequently, either (11a) is a maximum, (11b) being a minimum, or vice versa. In order to identify the maximum and the minimum, the sign of the term in brackets in (12) should be obtained. By dividing such term by Z_d, and rearranging the terms, one obtains the following positive result, i.e.,

$$Z_0^2\left\{\frac{\beta_d}{Z_d} - \frac{\beta_a}{Z_a}\right\} + Z_a\beta_a - Z_d\beta_d > 0 \tag{13}$$

Expression (13) is positive since $Z_d < Z_a$, $\beta_d > \beta_a$, and $Z_a\beta_a - Z_d\beta_d = 0$ (see Appendix). According to this, (12a) is positive and therefore (11a) is a minimum. However, since the sensitivity is negative, the absolute value of the sensitivity, the relevant parameter, exhibits a maximum for $\beta_d l = n \cdot \pi$, and a minimum for $\beta_d l = (2n + 1)\cdot\pi/2$ (indeed, the sensitivity is zero for this phase condition, as demonstrated in Appendix).

Apparently, in view of expression (11a), sensitivity increases by decreasing the characteristic impedance of the uncovered part of the sensing line, Z_a, and consequently Z_d (as far as both impedances appear in the denominator in the corresponding expressions). However, reducing the line impedance means enhancing the width of the line. This, in turn, tends to approach the impedance of the covered line to the one of the uncovered line, as well as the corresponding phase constants, and this seems to go against sensitivity optimization, according to (11a).

To determine whether Z_a (or Z_d) should be high or low, it is convenient to carry out a numerical analysis of expression (11a), where

$$\beta_a = \frac{\omega}{c}\sqrt{\varepsilon_{eff,a}} \tag{14}$$

and a similar expression applies to β_d, with the exception of the subindex a, which must be replaced with the subindex d. In (14), c is the speed of light in vacuum, $\varepsilon_{eff,a}(\varepsilon_{eff,d})$ is the effective dielectric constant of the uncovered (covered) line, and ω is the angular frequency. For the uncovered line, the effective dielectric constant is [41]

$$\varepsilon_{eff,a} = \frac{\varepsilon_r + 1}{2} + \frac{\varepsilon_r - 1}{2}F \tag{15}$$

where F is a geometry factor given by

$$F = \left(1 + 12\frac{h}{W_s}\right)^{-1/2} \tag{16a}$$

for $W_s/h \geq 1$, or by

$$F = \left(1 + 12\frac{h}{W_s}\right)^{-1/2} + 0.04\left(1 - \frac{W_s}{h}\right)^2 \tag{16b}$$

for $W_s/h < 1$, where W_s and h correspond to the strip width and the substrate thickness, respectively. The validity of (16) is subjected to the condition $t \ll h$, where t is the thickness of the metallic layer. For the covered line, the effective dielectric constant is given by

$$\varepsilon_{eff,d} = \frac{\varepsilon_r + \varepsilon_{r,d}}{2} + \frac{\varepsilon_r - \varepsilon_{r,d}}{2}F \tag{17}$$

provided the thickness h_d of the dielectric slab extends over the region of influence of the electromagnetic field generated by the line (i.e., the slab can be considered to be semi-infinite in the normal-to-sensor direction). In (17), the geometry factor F is also given by (16), and the value is identical to the one of the uncovered line section, and $\varepsilon_{r,d}$ is the dielectric constant of the slab.

Concerning the characteristic impedance of the covered line section, Z_d, assuming that $t \ll h$, it can be approximated by [41]

$$Z_d = \frac{\eta_0}{\sqrt{\varepsilon_{eff,d}}}\left\{\frac{W_s}{h} + 1.393 + 0.667\ln\left(\frac{W_s}{h} + 1.444\right)\right\}^{-1} \tag{18a}$$

for $W_s/h \geq 1$, where $\eta_0 = 120\pi\,\Omega$ is the characteristic impedance of vacuum, or by

$$Z_d = \frac{\eta_0}{2\pi\sqrt{\varepsilon_{eff,d}}}\ln\left(\frac{8h}{W_s} + \frac{W_s}{4h}\right) \tag{18b}$$

for $W_s/h < 1$. For Z_a, expressions (18) also apply, but $\varepsilon_{eff,d}$ must be replaced with $\varepsilon_{eff,a}$.

With expressions (14)-(18), the sensitivity (9) as a function of l (or $\beta_d l$) can be numerically calculated, and particularly the maximum value (corresponding to a phase of $\beta_d l = n \cdot \pi$) can be inferred. Figure 3 depicts the dependence of the sensitivity S_l with $\beta_d l$ for different values of the characteristic impedance of the uncovered and covered line sections. For that purpose, we have set the substrate thickness to a fixed value, $h = 1.524$ mm, and we have varied the width of the line, thereby modifying the characteristic impedances. According to Fig. 3, the maximum sensitivity (for $\beta_d l = n\cdot\pi$) increases by decreasing the impedance Z_a, or Z_d.

According to the previous words, the strategy for sensitivity optimization in the sensor merely consisting of the sensing line is clear. The phase of the covered line should be set to $\beta_d l = n \cdot \pi$, and the characteristic impedance, Z_d, or Z_a, must be small, as compared to the reference impedance of the ports. It is also necessary to use a movable slab with a relatively high dielectric constant, since this generates an

$$\rho_{in,a} = \frac{-Z_0(Z_a + Z_d\tan(\beta_a(l - l_d))\cot(\beta_d l_d)) + jZ_a(Z_a\tan(\beta_a(l - l_d)) - Z_d\cot(\beta_d l_d))}{+Z_0(Z_a + Z_d\tan(\beta_a(l - l_d))\cot(\beta_d l_d)) + jZ_a(Z_a\tan(\beta_a(l - l_d)) - Z_d\cot(\beta_d l_d))} \tag{4}$$

$$S_l = \frac{2\left\{-Z_dZ_0\beta_d + Z_aZ_0\beta_a\sin^2(\beta_d l) + Z_0Z_d^2Z_a^{-1}\beta_a\cos^2(\beta_d l)\right\}}{Z_0^2\sin^2(\beta_d l) + Z_d^2\cos^2(\beta_d l)} \tag{9}$$

$$\frac{dS_l}{dl} = \frac{4Z_dZ_0\beta_d\sin(\beta_d l)\cos(\beta_d l)\left\{(Z_aZ_d - Z_dZ_0^2Z_a^{-1})\beta_a + (Z_0^2 - Z_d^2)\beta_d\right\}}{\left\{Z_0^2\sin^2(\beta_d l) + Z_d^2\cos^2(\beta_d l)\right\}^2} \tag{10}$$

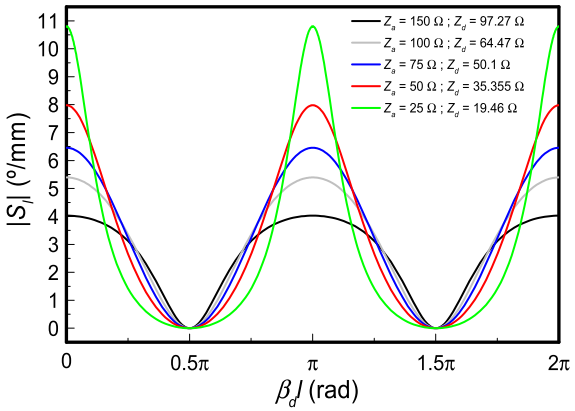

FIGURE 3. Sensitivity S_l as a function of $\beta_d l$ for different values of the characteristic impedance of the sensing line.

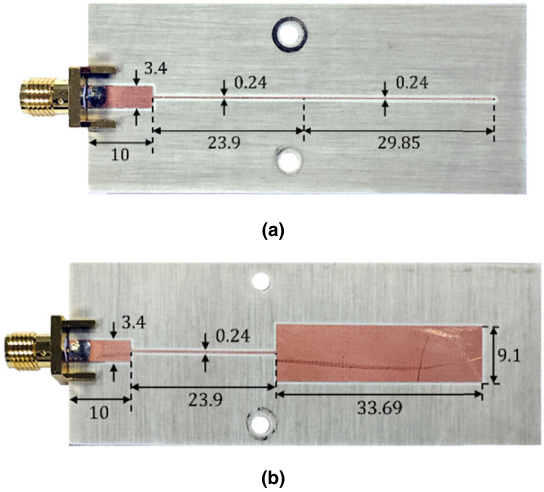

FIGURE 4. Photograph of the fabricated sensors, Sensor A (a) and B (b). Dimensions are given in mm.

appreciable difference between the characteristic impedances and phase constants of the uncovered and covered line sections.

Let us now analyze the sensor based on the step-impedance open-ended line of Fig. 2. The presence of the line section (design line) with impedance Z_1 and electrical length $\phi_1 = \beta_1 l_1$ (β_1 and l_1 being the phase constant and the line length, respectively) contributes to sensitivity enhancement, provided the line parameters are adequately chosen. In particular, let us consider that the electrical length of this line at the design frequency is $\phi_1 = 90°$. The impedance seen from the input port, Z_{in}, is thus

$$Z_{in} = \frac{Z_1^2}{Z_{in,a}} \tag{19}$$

and the reflection coefficient is

$$\rho = \frac{Z_1^2/Z_{in,a} - Z_0}{Z_1^2/Z_{in,a} + Z_0} \tag{20}$$

Let us now designate by $\chi_{in,a}$ the reactance of the sensing line, i.e., $Z_{in,a} = j\chi_{in,a}$. The reflection coefficient can be expressed as

$$\rho = \frac{Z_1^2/j\chi_{in,a} - Z_0}{Z_1^2/j\chi_{in,a} + Z_0} = \frac{Z_1^2 - j\chi_{in,a}Z_0}{Z_1^2 + j\chi_{in,a}Z_0} \tag{21}$$

and the phase of the reflection coefficient is thus

$$\phi_\rho = 2\arctan\left(-\frac{\chi_{in,a}}{Z_1^2/Z_0}\right) \tag{22}$$

From (3), the phase of the reflection coefficient seen from the sensing line can be expressed as

$$\phi_{\rho_{in,a}} = 2\arctan\left(-\frac{\chi_{in,a}}{Z_0}\right) \tag{23}$$

By comparing (22) and (23), it can be concluded that the sensitivity analysis carried out by considering only the sensing line can be applied to the sensor composed by the sensing line plus the quarter-wavelength ($\phi_1 = 90°$) transmission line. It suffices to replace Z_0 with Z_1^2/Z_0 in (11), provided (23) is identical to (22) with this change of variable.

According to the previous paragraph, for the step-impedance based sensor with $\beta_d l = n \cdot \pi$ and $\phi_1 = \pi/2$, the sensitivity is given by

$$S_l = 2\frac{Z_1^2}{Z_0}\left\{\frac{\beta_a}{Z_a} - \frac{\beta_d}{Z_d}\right\} \tag{24}$$

and by choosing the impedances according to $Z_1 > Z_0 > Z_a$ (or Z_d), with a high impedance contrast (i.e., $Z_1/Z_a \gg 1$), the sensitivity can be significantly optimized.

III. SENSOR DESIGN, FABRICATION AND VALIDATION

The design, fabrication and validation of two prototype displacement sensors are reported in this section. The difference concerns the characteristic impedances (covered and uncovered) of the 180° sensing lines. In one prototype sensor, Sensor A, $Z_d = 97.27\ \Omega$ and $Z_a = 150\ \Omega$, whereas in the prototype identified as Sensor B, $Z_d = 19.46\ \Omega$ and $Z_a = 25\ \Omega$. In both sensors, the cascaded 90° line exhibits a high characteristic impedance of $Z_1 = 150\ \Omega$ (the reference impedance of the port being $Z_0 = 50\ \Omega$). The operating frequency of the sensors is set to $f_0 = 2$ GHz. The sensors are implemented in the *Rogers RO4003C* substrate with dielectric constant $\varepsilon_r = 3.55$ and thickness $h = 1.524$ mm. The movable dielectric slab is an uncladded piece of the *Rogers RO3010* substrate with dielectric constant $\varepsilon_{r,d} = 10.2$ and thickness $h_d = 3.81$ mm (with such dielectric slab, the above indicated values of Z_d in both sensors result).

The photographs of the sensors are depicted in Fig. 4 (dimensions are indicated in the figure). Sensor fabrication has been carried out by means of the *LPKF H100* drilling machine. For sensor validation, the *Agilent N5221A* vector network analyzer has been used to obtain the phase of the reflection coefficient. Slab displacement over the sensing line has been carried out by means of the linear stepper motor (model *THORLABS LTS300/M*), available in our laboratory. The reference (REF) position is the one corresponding to the

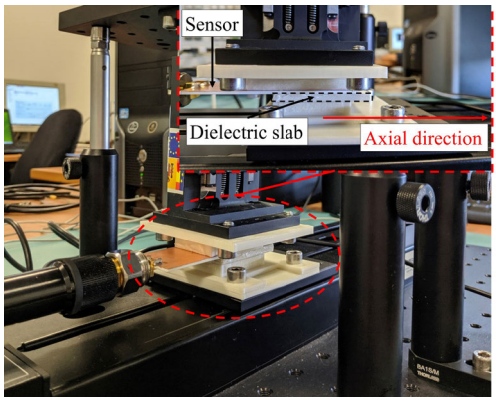

FIGURE 5. Photograph of the experimental setup for sensor validation.

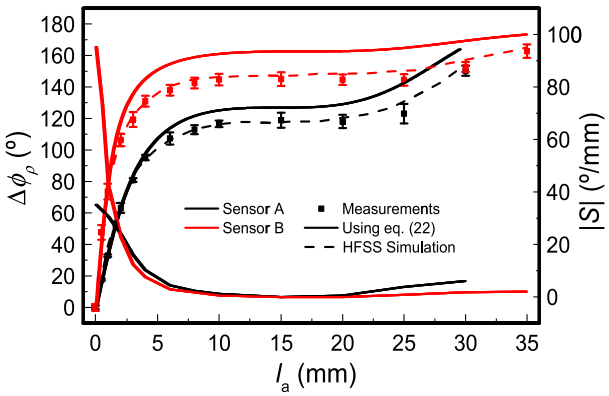

FIGURE 6. Dependence of the phase of the reflection coefficient with the slab displacement, and sensitivity, for sensors A (a) and B (b). For the measured data, error bars, corresponding to the standard deviation divided by the square root of the number of measurements that make up the mean (3 measurement points in our case), are depicted.

slab with its edge located in the step discontinuity (i.e., $l_a = 0$, or $l_d = l$, or $x = 0$). The picture of the experimental setup is shown in Fig. 5.

Fig. 6 shows the variation of the phase of the reflection coefficient in reference to the phase corresponding to the REF position, as a function of the slab displacement, l_a, for both sensors. The figure includes the measured data points, the phase inferred from the HFSS simulator, and the results predicted by the theory (expression 22). The figure depicts also the sensitivity, inferred by simple derivation of the experimental data points. The maximum sensitivity is found to be 35.14 °/mm and 95.24 °/mm for sensors A and B, respectively. Such maximum sensitivity is inferred when the slab is in the REF position, and should be coherent with the value predicted by expression (24). Evaluation of this expression for both sensors gives $|S_l| = 36.44$ °/mm and $|S_l| = 97.67$ °/mm for sensors A and B, respectively. These values coincide with the maximum sensitivities of Fig. 6 to a good approximation. Therefore, these simple calculations validate the analysis of the previous section. It should be mentioned that for the generation of the layout of the proposed sensor, the *Linecalc* tool of the *Keysight ADS* commercial software has been used. This software provides the width and length of the involved microstrip line sections, provided the substrate parameters and characteristic impedances are known. Nevertheless, dimension fine-tuning has been carried out with *Agilent Momentum*.

IV. DISCUSSION

According to (24), the sensitivity, a key parameter in any sensor, is mainly dictated by the impedance contrasts of the sensing line and the 90° line cascaded to it (both with regard to the reference impedance of the port). Depending on the required sensitivity, the necessary impedance contrasts may not be achievable. The reason is that very high line impedances require extremely narrow lines (not implementable if the line width is below the limits imposed by the technology in use). Conversely, very wide lines are necessary to achieve extremely low line impedances. However, an excessive line width should be avoided in order to prevent from parasitic effects related to the step discontinuity or the appearance of transverse resonances.

There is, however, an alternative approach to enhance the sensitivity, yet keeping the impedance contrasts at relatively small values. The idea is to cascade further 90° lines, with alternating characteristic impedances, to the sensing line. Let us consider that N 90°-lines are cascaded to the sensing line, and let us call Z_i the characteristic impedance of line section i, with $i = 1, 2, 3 \ldots N$. The input impedance can be expressed as

$$Z_{in,N} = Z_{in,a}^{(-1)^N} \cdot \prod_{i=1}^{N} \left\{ Z_i^{2\cdot(-1)^{i+N}} \right\} \tag{25}$$

or, using $Z_{in,a} = j\chi_{in,a}$

$$Z_{in,N} = j\,(-1)^N \chi_{in,a}^{(-1)^N} \cdot \prod_{i=1}^{N} \left\{ Z_i^{2\cdot(-1)^{i+N}} \right\} \tag{26}$$

where Π is the product operator. The reflection coefficient is thus

$$\rho = \frac{j\,(-1)^N \cdot \chi_{in,a}^{(-1)^N} \cdot \prod_{i=1}^{N} \left\{ Z_i^{2\cdot(-1)^{i+N}} \right\} - Z_0}{j\,(-1)^N \cdot \chi_{in,a}^{(-1)^N} \cdot \prod_{i=1}^{N} \left\{ Z_i^{2\cdot(-1)^{i+N}} \right\} + Z_0} \tag{27}$$

For N odd, the phase of the reflection coefficient is

$$\phi_\rho = 2\arctan\left(-\frac{\chi_{in,a}}{\prod_{i=1}^{N} \left\{ Z_i^{2\cdot(-1)^{i+N}} \right\} / Z_0} \right) \tag{28}$$

whereas for N even the phase is found to be

$$\phi_\rho = 2\arctan\left(-\frac{\chi_{in,a}}{Z_0 / \prod_{i=1}^{N} \left\{ Z_i^{2\cdot(-1)^{i+N}} \right\}} \right) \tag{29}$$

Thus, four situations arise, depending on the parity of N and the phase of $\beta_d l$, i.e.,

- For the sensing line satisfying $\beta_d l = n \cdot \pi$ and N odd, the sensitivity is

$$S_l = 2\frac{\prod_{i=1}^{N} \left\{ Z_i^{2\cdot(-1)^{i+N}} \right\}}{Z_0} \left\{ \frac{\beta_a}{Z_a} - \frac{\beta_d}{Z_d} \right\} \tag{30a}$$

- For $\beta_d l = n \cdot \pi$ and N even, the sensitivity is

$$S_l = 2\frac{Z_0}{\prod_{i=1}^{N}\left\{Z_i^{2\cdot(-1)^{i+N}}\right\}}\left\{\frac{\beta_a}{Z_a} - \frac{\beta_d}{Z_d}\right\} \quad (30b)$$

- For $\beta_d l = (2n+1)\cdot \pi/2$ and N odd, the sensitivity is

$$S_l = 2\frac{Z_0}{\prod_{i=1}^{N}\left\{Z_i^{2\cdot(-1)^{i+N}}\right\}}\left\{Z_a\beta_a - Z_d\beta_d\right\} \quad (30c)$$

- For $\beta_d l = (2n+1)\cdot \pi/2$ and N even, the sensitivity is

$$S_l = 2\frac{\prod_{i=1}^{N}\left\{Z_i^{2\cdot(-1)^{i+N}}\right\}}{Z_0}\left\{Z_a\beta_a - Z_d\beta_d\right\} \quad (30d)$$

Nevertheless, for $\beta_d l = (2n+1)\cdot \pi/2$, the sensitivity is null regardless of the parity of N, as far as $Z_a\beta_a - Z_d\beta_d = 0$, as demonstrated in Appendix. Thus, for sensitivity optimization, the phase of the sensing line should be set to $\beta_d l = n \cdot \pi$, the characteristic impedance of this line must be low, and the impedances of the subsequent cascaded lines must be alternately high and low. By this means, there is a multiplicative effect, and the sensitivity can be substantially enhanced without the need of implementing the lines with extreme impedances.

To demonstrate the sensitivity enhancement capability of the sensor by adding further 90° stages, we have simulated the sensor B of the previous section (Fig. 4b) by cascading a low impedance ($Z_2 = 25\ \Omega$) 90° line section to it (let us designate this sensor, with $N = 2$, as Sensor C). Like in Fig. 6, we have simulated the variation of the phase of the reflection coefficient in reference to the phase corresponding to the REF position, as a function of the slab displacement, l_a. The results are depicted in Fig. 7. This figure includes also the sensitivity, which exhibits the maximum value for the REF position. The maximum sensitivity inferred from simulation (312.97 °/mm) is somehow smaller than the value predicted by the theory, given by expression (30b), i.e., 390.83 °/mm. This relatively small discrepancy is because with such very high sensibility it is very difficult to accurately infer the sensitivity from the derivative of the phase data points. Nevertheless, it is clear that the sensitivity is substantially enhanced by adding the low impedance 90° line section to sensor B, resulting in a highly sensitive Sensor C.

It should be emphasized that the sensitivity analysis carried out in this paper refers to S_l, the sensitivity in the limit of small displacements with regard to the REF position (with $x = 0$). This sensitivity is maximized if the sensor is designed according to the given design guidelines. Nevertheless, the sensitivity decreases as the displacement increases, as it can be appreciated in Figs. 6 and 7, where the sensitivity S as a function of the displacement can be observed. According to these figures, it is clear that the proposed sensors are especially useful for the measurement of small displacements in the vicinity of the REF position, where the phase of the reflection coefficient, the output variable, experiences a stronger variation with the displacement of the slab. Sensitivity enhancement is achieved

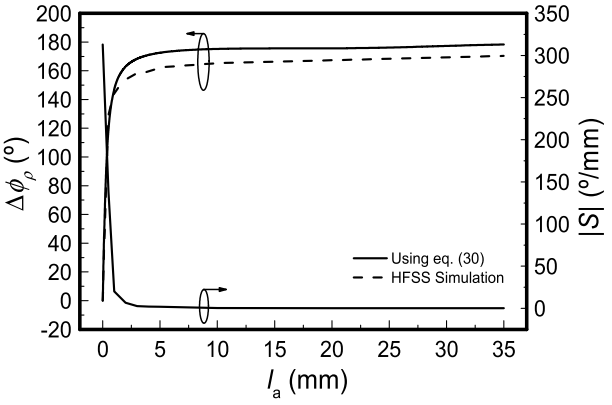

FIGURE 7. Dependence of the phase of the reflection coefficient with the slab displacement, and sensitivity, for sensor C (described in the text).

at the expense of a reduced input dynamic range, as visible in the quasi-saturation effect of Figs. 6 and 7. However, the results of Figs. 6 and 7 and the analysis of this section demonstrate that the sensitivity for small displacements can be enhanced at wish by merely adding 90° line sections with alternating high and low impedance. Thus, these sensors are indicated in applications where small linear displacements need to be measured.

One potential application of these sensors may be the accurate measurement of liquid levels. Although this specific application is left for future investigation and it is out of the scope of this paper, it is convenient to analyze the effects of the dielectric constant of the movable slab on the sensor sensitivity. In particular, since the dielectric constant of liquids at microwave frequencies is high, it is convenient to simulate one of the sensors (for example, Sensor B, with $N = 1$) by considering a high dielectric constant slab. A high dielectric constant slab increases the impedance contrast and the phase constant contrast between the covered and uncovered sections of the sensing line. Therefore, according to expression (24), it is expected that the sensitivity increase with the dielectric constant of the movable slab. This aspect is demonstrated in Fig. 8, where the simulation of Sensor B by considering slabs of high ($\varepsilon_{r,d} = 30$) and low ($\varepsilon_{r,d} = 2$) dielectric constant are considered. It should be mentioned, however, that the sensor B has been redesigned in each case, to account for the variation of the physical length of the sensing line, necessary to achieve the required phase of 180° (thereby optimizing the maximum sensitivity) when a semi-infinite slab of the indicated dielectric constants covers it. Thus, the width of the sensing lines are $W_s = 9.1$ mm and the lengths for $\varepsilon_{r,d} = 30$ and for $\varepsilon_{r,d} = 2$ are $l = 24.77$ mm and $l = 41.75$ mm, respectively. In view of Fig. 8, it is confirmed that the maximum sensitivity increases with the dielectric constant of the movable slab, as expected (the vertical scale in Fig. 8 is identical to the one of Fig. 6 to ease the comparison).

Naturally, increasing the thickness of the slabs enhances also the maximum sensitivity due to identical reasons (further contrast of the phase constant and characteristic impedance

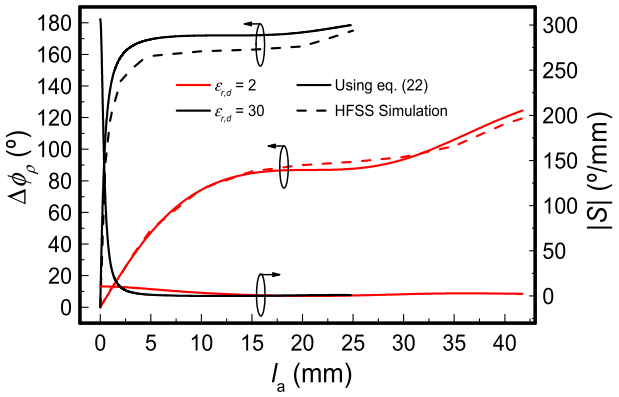

FIGURE 8. Dependence of the phase of the reflection coefficient with the slab displacement, and sensitivity, for modified sensor B, with the movable slab of the indicated dielectric constants.

TABLE 1. Comparison of various planar microwave linear displacement sensors.

Ref.	*Frequency range (GHz)*	*Sensitivity*	*Resolution*
[1]	2.35-2.55	0.1 GHz/mm	100 μm
[2]	6.0-10.0	1.2 GHz/mm	8.3 μm
[5]	6.0-6.9	0.2 GHz/mm	50 μm
[6]	1.7-4.3	0.5 GHz/mm	20 μm
[8]	2.0	65 dB/mm	46 μm
[9]	1.13	25 dB/mm	120 μm
[13]	4.25	18.7 dB/mm	160 μm
[21]	4.1	---	600 μm
[22]	3.9	---	3,400 μm
[Sensor A]	**2.0**	**35.14°/mm**	**142.2 μm**
[Sensor B]	**2.0**	**95.24°/mm**	**52.4 μm**
[Sensor C]	**2.0**	**312.97°/mm**	**15.9 μm**

between the covered and uncovered sensing line sections). However, in this paper, the considered thickness of the slabs (3.81 mm) is sufficient to consider them semi-infinite in the vertical direction (so that the electromagnetic field generated by the line does not reach the slab/air interface). That is, further enhancing this thickness does not modify the sensitivity (as it has been verified by independent simulations, not shown).

To end this section, let us mention that sensor sensitivity can also be enhanced by increasing the operating frequency. This is apparent in view of expressions (11), (24) and (30), since the phase constants of the covered and uncovered line are proportional to the operating frequency. The value considered in the present paper ($f_0 = 2$ GHz) obeys a tradeoff between sensor size (smaller as higher the frequency), sensitivity, and ease of measurement.

V. COMPARISON WITH OTHER LINEAR DISPLACEMENT SENSORS

Comparing the proposed reflective-mode phase-variation linear displacement sensors with other planar microwave displacement sensors is not easy. The reason is that in most microwave sensors devoted to the measurement of spatial variables, the output variable is typically a resonance frequency, a magnitude (of either a transmission or a reflection coefficient), a voltage amplitude, or a cumulative number of pulses, rather than a phase. Exceptions are the phase-variation sensors reported in [28], [29], but such sensors are devoted to the measurement of angular, rather than linear, displacements and velocities.

Table 1 shows a comparison of various linear displacement sensors reported in the recent literature. It can be appreciated that in the coupling modulation sensors [8], [9], [13], pulse-counting sensors [21], [22], as well as in the sensors reported in this work (sensors A, B and C), the required signal for sensing is a single-tone (harmonic) signal, this representing a clear advantage over the frequency-variation sensors [1], [2], [5], [6], as discussed before. Concerning sensor resolution, it has been considered that for the frequency variation sensors [1], [2], [5], [6], the system is able to discern frequency variations of 10 MHz (an optimistic value), thereby providing the input resolution values given in the table. For the coupling modulation sensors, the input resolution has been inferred by considering that 3 dB in the output variable (a transmission coefficient) can be discerned. For the sensors proposed in this work, it is assumed that phase variations of 5° can be resolved with any reasonable instrument. According to it, and taking into account the maximum sensitivities given in Table 1, the indicated displacement resolutions are obtained. These resolutions are competitive, as consequence of the high sensitivity, especially for sensor C. It should be mentioned that for the sensors based on cumulative pulse counting [21], [22], based on chains of inclusions (metallic strips in [21] and dielectric strips in [22]), the resolution is dictated by the period of the inclusions' chain. Such period is relatively high, thereby providing poor resolution as compared to the other sensors reported in the table. However, the sensors in [21], [22] are devoted to the measurement of high range displacements (typically dozens of mm, or even more), contrary to the other sensors in Table 1 (with input linear dynamic ranges of few mm or even less). For this reason, the sensor resolutions reported in [21], [22] (in the millimeter range) are considered to be competitive, as well.

Concerning the input dynamic range with linear response of the sensors reported in this paper, it is apparent that such range is degraded by increasing the sensitivity. However, a high sensitivity is typically required in applications where small displacements should be detected. If the measuring displacement range needs to be expanded, it should be convenient to reduce the maximum sensitivity in order to improve the sensor linearity.

VI. CONCLUSION

In conclusion, a microwave sensor devoted to the measurement of small displacements has been reported in this paper. The sensor is composed of a static part, an open-ended

step-impedance microstrip line, and a movable part, a dielectric slab. The sensor operates in reflection, and the output variable is the phase of the reflection coefficient, which varies as the dielectric slab moves along the open-ended (sensing) line on top of it. It has been demonstrated that for sensitivity optimization, the electrical length of the open-ended sensing line covered by the dielectric slab must be $n \cdot \pi$, n being an integer number, and the impedance of the sensing line must be low. By cascading additional quarter-wavelength transmission line sections between the sensing line and the input port, with alternating high and low impedance (thereby forming a step-impedance open-ended line), the sensitivity is substantially enhanced. Two prototype devices, consisting of a 180° open-ended sensing line cascaded to a high impedance 90° line, have been designed and fabricated. In one of them, the impedance of the sensing line is low, whereas it is high in the other one. The achieved maximum sensitivity has been found to be 95.24 °/mm and 35.14 °/mm for the sensor with low and high impedance sensing line, respectively. These results validate the theory and point out the potential for sensitivity optimization. Nevertheless, the sensitivity can be further enhanced if required, by simply cascading additional 90° lines with alternating high and low impedance. This sensitivity enhancement has been demonstrated at simulation level by considering a further sensor design consisting of a 180° sensing line plus two cascaded 90° line sections with alternating high/low impedance (the achieved sensitivity has been found to be 312.97 °/mm in this case). Besides the high achievable sensitivity, the proposed sensor is very simple (i.e., a one-port high/low step-impedance open-ended line), it can easily be fabricated, it operates at a single frequency, and it is robust against noise effects, as far as its working principle is phase variation.

APPENDIX

To demonstrate that the term in brackets in (11b) is null, note that the impedance of the covered and uncovered sensing line can be expressed as

$$Z_d = \frac{Z}{\sqrt{\varepsilon_{eff,d}}} \tag{A.1a}$$

$$Z_a = \frac{Z}{\sqrt{\varepsilon_{eff,a}}} \tag{A.1b}$$

where Z is given by (18) excluding the square root of the effective dielectric constant. The phase constants, β_a and β_d, are given by (14), with the convenient sub-index in the effective dielectric constant. Since the square root of the effective dielectric constant appears in the numerator in the phase constant, and it appears in the denominator in the characteristic impedance, the product $Z_a\beta_a$ or $Z_d\beta_d$does not depend on the material on top of the sensing line. Indeed, in both cases the following result is obtained

$$\beta_a Z_a = \beta_d Z_d = \frac{Z\omega}{c} \tag{A.2}$$

Consequently, $Z_a\beta_a - Z_d\beta_d = 0$, and the sensitivity for $\beta_d l = (2n+1)\cdot\pi/2$, given by (11b), is $S_l = 0$.

REFERENCES

[1] C. Mandel, B. Kubina, M. Schüßler, and R. Jakoby, "Passive chipless wireless sensor for two-dimensional displacement measurement," in *Proc. 41st Eur. Microw. Conf.*, Manchester, U.K., 2011, pp. 79–82.

[2] M. Rezaee and M. Joodaki, "Two-dimensional displacement sensor based on CPW line loaded by defected ground structure with two separated transmission zeroes," *IEEE Sensors J.*, vol. 17, no. 4, pp. 994–999, Feb. 2017.

[3] A. Maleki Gargari, B. Ozbey, H. V. Demir, A. Altintas, U. Albostan, O. Kurc, and V. B. Erturk, "A wireless metamaterial-inspired passive rotation sensor with submilliradian resolution," *IEEE Sensors J.*, vol. 18, no. 11, pp. 4482–4490, Jun. 2018.

[4] A. K. Jha, N. Delmonte, A. Lamecki, M. Mrozowski, and M. Bozzi, "Design of microwave-based angular displacement sensor," *IEEE Microw. Wireless Compon. Lett.*, vol. 29, no. 4, pp. 306–308, Apr. 2019.

[5] Y. Tian, J. Wu, L. Yu, H. Yang, and X. Huang, "Ultrasensitive displacement sensor based on tunable horn-shaped resonators," *Smart Mater. Struct.*, vol. 27, no. 4, Apr. 2018, Art. no. 045013.

[6] M. Abdolrazzaghi and M. Daneshmand, "Multifunctional ultrahigh sensitive microwave planar sensor to monitor mechanical motion: Rotation, displacement, and stretch," *Sensors*, vol. 20, no. 4, p. 1184, Feb. 2020.

[7] J. Naqui, M. Durán-Sindreu, and F. Martín, "Novel sensors based on the symmetry properties of split ring resonators (SRRs)," *Sensors*, vol. 11, no. 8, pp. 7545–7553, Jul. 2011.

[8] J. Naqui, M. Durán-Sindreu, and F. Martín, "Alignment and position sensors based on split ring resonators," *Sensors*, vol. 12, no. 9, pp. 11790–11797, Aug. 2012.

[9] A. K. Horestani, C. Fumeaux, S. F. Al-Sarawi, and D. Abbott, "Displacement sensor based on diamond-shaped tapered split ring resonator," *IEEE Sensors J.*, vol. 13, no. 4, pp. 1153–1160, Apr. 2013.

[10] A. K. Horestani, D. Abbott, and C. Fumeaux, "Rotation sensor based on horn-shaped split ring resonator," *IEEE Sensors J.*, vol. 13, no. 8, pp. 3014–3015, Aug. 2013.

[11] J. Naqui and F. Martin, "Transmission lines loaded with bisymmetric resonators and their application to angular displacement and velocity sensors," *IEEE Trans. Microw. Theory Techn.*, vol. 61, no. 12, pp. 4700–4713, Dec. 2013.

[12] J. Naqui and F. Martin, "Angular displacement and velocity sensors based on electric-LC (ELC) loaded microstrip lines," *IEEE Sensors J.*, vol. 14, no. 4, pp. 939–940, Apr. 2014.

[13] A. K. Horestani, J. Naqui, F. Martín, C. Fumeaux, and D. Abbott, "Two-dimensional displacement and alignment sensor based on reflection coefficients of open microstrip lines loaded with split ring resonators," *Electron. Lett.*, vol. 50, no. 8, pp. 620–622, Apr. 2014.

[14] A. Ebrahimi, W. Withayachumnankul, S. F. Al-Sarawi, and D. Abbott, "Metamaterial-inspired rotation sensor with wide dynamic range," *IEEE Sensors J.*, vol. 14, no. 8, pp. 2609–2614, Aug. 2014.

[15] J. Naqui, J. Coromina, A. Karami-Horestani, C. Fumeaux, and F. Martín, "Angular displacement and velocity sensors based on coplanar waveguides (CPWs) loaded with S-Shaped split ring resonators (S-SRR)," *Sensors*, vol. 15, no. 5, pp. 9628–9650, Apr. 2015.

[16] F. Martin, *Artificial Transmission Lines for RF and Microwave Applications*. Hoboken, NJ, USA: Wiley, 2015.

[17] J. Naqui, *Symmetry Properties in Transmission Lines Loaded With Electrically Small Resonators: Circuit Modeling and Applications*. Cham, Switzerland: Springer, 2016.

[18] J. Mata-Contreras, C. Herrojo, and F. Martin, "Application of split ring resonator (SRR) loaded transmission lines to the design of angular displacement and velocity sensors for space applications," *IEEE Trans. Microw. Theory Techn.*, vol. 65, no. 11, pp. 4450–4460, Nov. 2017.

[19] C. Herrojo, J. Mata-Contreras, F. Paredes, and F. Martin, "Microwave encoders for chipless RFID and angular velocity sensors based on S-shaped split ring resonators," *IEEE Sensors J.*, vol. 17, no. 15, pp. 4805–4813, Aug. 2017.

[20] J. Mata-Contreras, C. Herrojo, and F. Martin, "Detecting the rotation direction in contactless angular velocity sensors implemented with rotors loaded with multiple chains of resonators," *IEEE Sensors J.*, vol. 18, no. 17, pp. 7055–7065, Sep. 2018.

[21] C. Herrojo, F. Paredes, and F. Martin, "Double-stub loaded microstrip line reader for very high data density microwave encoders," *IEEE Trans. Microw. Theory Techn.*, vol. 67, no. 9, pp. 3527–3536, Sep. 2019.

[22] C. Herrojo, F. Paredes, J. Bonache, and F. Martin, "3-D-Printed high data-density electromagnetic encoders based on permittivity contrast for motion control and chipless-RFID," *IEEE Trans. Microw. Theory Techn.*, vol. 68, no. 5, pp. 1839–1850, May 2020.
[23] C. Herrojo, M. Moras, F. Paredes, A. Nunez, J. Mata-Contreras, E. Ramon, and F. Martin, "Time-domain-signature chipless RFID tags: Near-field chipless-RFID systems with high data capacity," *IEEE Microw. Mag.*, vol. 20, no. 12, pp. 87–101, Dec. 2019.
[24] F. Martin, C. Herrojo, J. Mata-Contreras, and F. Paredes, *Time-Domain Signature Barcodes for Chipless-RFID and Sensing Applications*. Cham, Switzerland: Springer, 2020.
[25] F. Ferrández-Pastor, J. García-Chamizo, and M. Nieto-Hidalgo, "Electromagnetic differential measuring method: Application in microstrip sensors developing," *Sensors*, vol. 17, no. 7, p. 1650, Jul. 2017.
[26] J. Munoz-Enano, P. Velez, M. Gil Barba, and F. Martin, "An analytical method to implement high-sensitivity transmission line differential sensors for dielectric constant measurements," *IEEE Sensors J.*, vol. 20, no. 1, pp. 178–184, Jan. 2020.
[27] J. Munoz-Enano, P. Velez, M. Gil Barba, J. Mata-Contreras, and F. Martin, "Differential-mode to common-mode conversion detector based on rat-race hybrid couplers: Analysis and application to differential sensors and comparators," *IEEE Trans. Microw. Theory Techn.*, vol. 68, no. 4, pp. 1312–1325, Apr. 2020.
[28] A. K. Jha, A. Lamecki, M. Mrozowski, and M. Bozzi, "A highly sensitive planar microwave sensor for detecting direction and angle of rotation," *IEEE Trans. Microw. Theory Techn.*, vol. 68, no. 4, pp. 1598–1609, Apr. 2020.
[29] A. K. Horestani, Z. Shaterian, and F. Martin, "Rotation sensor based on the cross-polarized excitation of split ring resonators (SRRs)," *IEEE Sensors J.*, vol. 20, no. 17, pp. 9706–9714, Sep. 2020.
[30] A. M. Albishi, M. K. E. Badawe, V. Nayyeri, and O. M. Ramahi, "Enhancing the sensitivity of dielectric sensors with multiple coupled complementary split-ring resonators," *IEEE Trans. Microw. Theory Techn.*, vol. 68, no. 10, pp. 4340–4347, Oct. 2020, doi: 10.1109/TMTT.2020.3002996.
[31] M. Abdolrazzaghi, M. Daneshmand, and A. K. Iyer, "Strongly enhanced sensitivity in planar microwave sensors based on metamaterial coupling," *IEEE Trans. Microw. Theory Techn.*, vol. 66, no. 4, pp. 1843–1855, Apr. 2018.
[32] A. Javed, A. Arif, M. Zubair, M. Qasim Mehmood, and K. Riaz, "A low-cost multiple complementary split-ring resonator-based microwave sensor for contactless dielectric characterization of liquids," *IEEE Sensors J.*, vol. 20, no. 19, pp. 11326–11334, Oct. 2020.
[33] A. Ebrahimi, J. Scott, and K. Ghorbani, "Transmission lines terminated with LC resonators for differential permittivity sensing," *IEEE Microw. Wireless Compon. Lett.*, vol. 28, no. 12, pp. 1149–1151, Dec. 2018.
[34] A. Ebrahimi, J. Scott, and K. Ghorbani, "Microwave reflective biosensor for glucose level detection in aqueous solutions," *Sens. Actuators A, Phys.*, vol. 301, Jan. 2020, Art. no. 111662.
[35] J. Muñoz-Enano, P. Vélez, M. Gil, and F. Martín, "Microfluidic reflective-mode differential sensor based on open split ring resonators (OSRRs)," *Int. J. Microw. Wireless Technol.*, vol. 12, no. 7, pp. 588–597, Sep. 2020.
[36] J. Munoz-Enano, P. Velez, L. Su, M. Gil, P. Casacuberta, and F. Mart, "On the sensitivity of reflective-mode phase-variation sensors based on open-ended stepped-impedance transmission lines: Theoretical analysis and experimental validation," *IEEE Trans. Microw. Theory Techn.*, early access, Sep. 25, 2020, doi: 10.1109/TMTT.2020.3023728.
[37] V. Sipal, A. Z. Narbudowicz, and M. J. Ammann, "Contactless measurement of angular velocity using circularly polarized antennas," *IEEE Sensors J.*, vol. 15, no. 6, pp. 3459–3466, Jun. 2015.
[38] A. H. Karami, F. K. Horestani, M. Kolahdouz, and A. K. Horestani, "Rotation sensor based on magnetic microrods," *IEEE Sensors J.*, vol. 18, no. 1, pp. 77–82, Jan. 2018.
[39] A. H. Karami, F. Karami Horestani, M. Kolahdouz, A. K. Horestani, and F. Martín, "2D rotary sensor based on magnetic composite of microrods," *J. Mater. Sci., Mater. Electron.*, vol. 31, no. 1, pp. 167–174, Jan. 2020.
[40] C.-H. Chio, R. Gomez-Garcia, L. Yang, K.-W. Tam, W.-W. Choi, and S.-K. Ho, "An angular-displacement microwave sensor using an unequal-length-Bi-path transversal filtering section," *IEEE Sensors J.*, vol. 20, no. 2, pp. 715–722, Jan. 2020.
[41] D. M. Pozar, *Microwave Engineering*, 4th ed. Hoboken, NJ, USA: Wiley, 2011.

JONATHAN MUÑOZ-ENANO (Graduate Student Member, IEEE) was born in Mollet del Vallès, Barcelona, Spain, in 1994. He received the bachelor's degree in electronic telecommunications engineering and the master's degree in telecommunications engineering from the Autonomous University of Barcelona (UAB), in 2016 and 2018, respectively. He is currently working with UAB in the elaboration of his Ph.D. degree, which is focused on the development of microwave sensors based on metamaterials concepts for the dielectric characterization of materials and biosensors.

PARIS VÉLEZ (Member, IEEE) was born in Barcelona, Spain, in 1982. He received the degree in telecommunications engineering, specializing in electronics, the Electronics Engineering degree, and the Ph.D. degree in electrical engineering from the Universitat Autònoma de Barcelona, Barcelona, in 2008, 2010, and 2014, respectively. His Ph.D. thesis concerned common mode suppression differential microwave circuits based on metamaterial concepts and semi-lumped resonators. During the Ph.D., he was awarded with a pre-doctoral teaching and research fellowship by the Spanish Government from 2011 to 2014. From 2015 to 2017, he was involved in the subjects related to metamaterials sensors for fluidics detection and characterization at LAAS-CNRS through a TECNIOSpring fellowship cofounded by the Marie Curie program. His current research interests include the miniaturization of passive circuits RF/microwave and sensors-based metamaterials through Juan de la Cierva fellowship. He is a Reviewer for the IEEE TRANSACTIONS ON MICROWAVE THEORY AND TECHNIQUES and for other journals.

LIJUAN SU was born in Qianjiang, Hubei, China, in 1983. She received the B.S. degree in communication engineering and the M.S. degree in circuits and systems from the Wuhan University of Technology, Wuhan, China, in 2005 and 2013, respectively, and the Ph.D. degree in electronic engineering from the Universitat Autonoma de Barcelona, Barcelona, Spain, in 2017. From November 2017 to December 2019, she worked as a Postdoctoral Researcher with the Flexible Electronics Research Center, Huazhong University of Science and Technology, Wuhan. She is currently a Postdoctoral Researcher with CIMITEC, Universitat Autònoma de Barcelona. Her current research interests include the development of novel microwave sensors with improved performance for biosensors, dielectric characterization of solids and liquids, defect detection, and industrial processes.

MARTA GIL-BARBA (Member, IEEE) was born in Valdepeñas, Ciudad Real, Spain, in 1981. She received the degree in physics from the Universidad de Granada, Spain, in 2005, and the Ph.D. degree in electronic engineering from the Universitat Autònoma de Barcelona, Barcelona, Spain, in 2009. She studied one year with the Friedrich Schiller Universität Jena, Jena, Germany. During her Ph.D. Thesis, she was holder of a METAMORPHOSE NoE Grant and a National Research Fellowship from the FPU Program of the Education and Science Spanish Ministry. As a Postdoctoral Researcher, she was awarded with a Juan de la Cierva fellowship working with the Universidad de Castilla-La Mancha. She was a Postdoctoral Researcher with the Institut für Mikrowellentechnik und Photonik, Technische Universität Darmstadt, and with the Carlos III University of Madrid. She is currently an Assistant Professor with the Universidad Politécnica de Madrid. She has worked in metamaterials, piezoelectric MEMS, and microwave passive devices. Her current interest includes metamaterials sensors for fluidic detection.

FERRAN MARTÍN (Fellow, IEEE) was born in Barakaldo, Vizcaya, Spain, in 1965. He received the B.S. degree in physics from the Universitat Autònoma de Barcelona (UAB), in 1988, and the Ph.D. degree in 1992.

From 1994 to 2006, he was an Associate Professor in Electronics with the Departament d'Enginyeria Electrònica, Universitat Autònoma de Barcelona, where he has been a Full Professor of Electronics, since 2007. In recent years, he has been involved in different research activities including modeling and simulation of electron devices for high-frequency applications, millimeter wave and THz generation systems, and the application of electromagnetic bandgaps to microwave and millimeter wave circuits. He is currently very active in the field of metamaterials and their application to the miniaturization and optimization of microwave circuits and antennas. He is also the Head of the Microwave Engineering, Metamaterials and Antennas Group (GEMMA Group), UAB, and the Director of CIMITEC, a research Center on Metamaterials supported by TECNIO (Generalitat de Catalunya). He has organized several international events related to metamaterials and related topics, including Workshops at the IEEE International Microwave Symposium in 2005 and 2007, European Microwave Conference in 2009, 2015, and 2017, and the Fifth International Congress on Advanced Electromagnetic Materials in Microwaves and Optics (Metamaterials 2011), where he acted as the Chair of the Local Organizing Committee. He has authored or coauthored more than 600 technical conference, letter, journal articles and book chapters, he is a coauthor of the book on Metamaterials *Metamaterials with Negative Parameters: Theory, Design, and Microwave Applications* (John Wiley & Sons Inc.), author of the book *Artificial Transmission Lines for RF and Microwave Applications* (John Wiley & Sons Inc.), co-editor of the book *Balanced Microwave Filters* (Wiley/IEEE Press), and coauthor of the book *Time-Domain Signature Barcodes for Chipless-RFID and Sensing Applications* (Springer). He has generated 21 Ph.D. students, has filed several patents on metamaterials and has headed several Development Contracts. His research interests include microwave sensors and RFID systems, with special emphasis on the development of high-data capacity chipless-RFID tags.

Dr. Martín is a Fellow of the IET. He is a member of the IEEE Microwave Theory and Techniques Society (IEEE MTT-S). He is a Reviewer of the IEEE TRANSACTIONS ON MICROWAVE THEORY AND TECHNIQUES and IEEE MICROWAVE AND WIRELESS COMPONENTS LETTERS, and among many other journals. He serves as a member of the Editorial Board of *IET Microwaves, Antennas, and Propagation*, *International Journal of RF and Microwave Computer-Aided Engineering*, and *Sensors*. He is also a member of the Technical Committees of the European Microwave Conference (EuMC) and International Congress on Advanced Electromagnetic Materials in Microwaves and Optics (Metamaterials). Among his distinctions, he has received the 2006 Duran Farell Prize for Technological Research, he holds the *Parc de Recerca UAB −− Santander* Technology Transfer Chair. He was a recipient of three ICREA ACADEMIA awards (calls 2008, 2013, and 2018). He has acted as a Guest Editor of six Special Issues on metamaterials and sensors in five International Journals.